



Investigating inhibition characteristics of *Butea monosperma* leaf extracts to retard stainless steel biocorrosion in the presence of sulfate-reducing bacteria

SHIV KUMAR MANU, NOYEL VICTORIA SELVAM
and MANIVANNAN RAMACHANDRAN*

Department of Chemical Engineering, National Institute of Technology Raipur,
Chhattisgarh – 492010, India

(Received 30 December 2022, revised 10 January, accepted 12 May 2023)

Abstract: The influence of sulfate-reducing bacteria *Desulfovibrio desulfuricans* on stainless steel SS 202 corrosion in neutral media was studied in detail using weight loss and electrochemical routes. The bacterial activity resulted in material loss with an average rate of 0.015 mm/year. The scanning electron microscopy (SEM) analysis showed a significant increase in the sessile bacterial population with the immersion period. Use of 500 ppm palash (*Butea monosperma*) leaf extract (PLE) reduced the average corrosion rate to 0.002 mm/year. SEM analysis showed a very thin external film formation in the presence of the inhibitor. The X-ray photoelectron spectroscopy studies confirmed the presence of corrosion products such as Fe₂O₃ and FeS. The gas chromatography–mass spectrometry studies showed the dominant percentage of various terpenoids along with vitamin E as the main components of the PLE. Electrochemical analysis showed the existence of a diffusion barrier. The resistance offered by the diffusion barrier is high in the inhibited sample when compared to uninhibited samples.

Keywords: biocorrosion; *Butea monosperma*; electrochemical study; X-ray photoelectron spectroscopy.

INTRODUCTION

The presence of bacteria in the environment surrounding a metal structure leads to its destruction by the corrosive products generated of their metabolic activity. This negative effect is frequently referred as biocorrosion or microbially influenced corrosion (MIC). Biocorrosion is caused by a wide variety of micro-organisms ranging from bacteria, algae and fungi.¹ MIC is prevalent in many process utilities and often leads to equipment breakdown, resulting in severe fin-

* Corresponding author. E-mail: rmani.che@nitrr.ac.in
<https://doi.org/10.2298/JSC221230026M>

ancial losses.¹ Corrosion caused by aggressive chemicals is widespread in all process plants and it can be identified, understood, and controlled with less difficulty. It is difficult to understand and control the MIC because of the interdependent activities of many microbes that change with local environmental factors involved in the MIC.²

Though the incidence percentage of MIC is not as high as chemical corrosion, 20 % of the total corrosion cost in any process unit is due to MIC.¹ It is well known that the effects of sulfate-reducing bacteria (SRB) are severe when compared to other bacterial species. The products of SRB metabolism are conducive and enhance the corrosion processes. The products of their metabolism produce corrosive polysulfides and sulfur that react with the metal ions leading to the production of respective metal sulfides which in turn are conducive and promote the formation of localized concentration cells to enhance corrosion and pitting.²

Stainless steel grade SS202 is widely used in many industrial applications, especially in the food industry. The characteristic feature of stainless steel is its corrosion-resistant properties. However, under aggressive environments, stainless steel is prone to corrosion. Inhibitors are playing an effective role in shielding metal substrates against corrosion. Despite their high efficiency, synthetic corrosion inhibitors cannot be employed regularly for corrosion prevention due to their severe environmental impacts. As a result, scientists have concentrated their efforts on developing green corrosion inhibitors. Plants, fruits, and their peels are excellent sources of phytochemical compounds that are less expensive and environmentally safer than the synthetic type of inhibitor.

Plant-based compounds contain certain natural compounds (phenolics compounds, lectins, essential oils, alkaloids, polypeptides, terpenoids and polyacetylenes) with powerful anti-biofilm properties.³ These phytochemical compounds work on bacteria by substrate deprivation, rupture of microbe membrane, preventing bacterial attachment on surfaces, affecting the metabolism of exopolymeric substance formation, and inducing mutations.^{4,5} The efficacy of Palash (*Butea monosperma*) leaf extract as green corrosion inhibitor on mild steel corrosion in 1 M HCl was studied and reported 96 % of corrosion inhibition efficiency.⁶ The palash leaf extract has antibacterial activity against microbes including *Escherichia coli*, *Pseudomonas aeruginosa* and *Staphylococcus aureus* due to the presence of active substances like sterols, triterpenes, glycosides, flavonoids and proteins.⁷ However, information on antibacterial activity against *Desulfovibrio desulfuricans* is not available in the literature. Hence, this is the first work reporting the antibacterial activity of palash leaf extract on *D. desulfuricans*. Tao *et al.* studied the role of total flavonoids of *Potentilla kleiniana* (TFP) against the stainless steel biocorrosion caused by *P. aeruginosa* bacterium by disrupting *P. aeruginosa*'s cell membrane.⁸ Lekbach *et al.* studied the efficiency of catechin

hydrate as biocorrosion inhibitor caused by *P. aeruginosa* in 304L stainless steel and obtained a maximum inhibition efficiency of 99 %.⁹

The present work reports detailed studies on *D. desulfuricans*-induced corrosion in SS 202 and control of the same using 500 ppm (palash leaves) extract.

EXPERIMENTAL

In this investigation, *Desulfovibrio desulfuricans* sp. strains (NCIM, Pune, India) were employed. The modified Baar's medium consists of K₂HPO₄-0.5 g, NH₄Cl-1.0 g, CaSO₄-2.0 g, MgSO₄·7H₂O-2.0 g, sodium lactate-7.0 g, Fe(NH₄)₂(SO₄)₂-0.5 g in 1000 ml distilled water. The pH of the medium used for the studies was 7. Stainless steel coupons (SS 202) were cut to a size of 1 cm×1 cm×0.05 cm, and polished well. One side of the polished samples was sealed with Teflon tape. For the electrochemical studies, a copper contact was attached to the sealed surface and this was used as the working electrode. The composition of stainless-steel coupons used in this study was as follows (wt. %): 0.18 C, 0.53 Si, 9.48 Mn, 0.075 P, 0.012 S, 13.71 Cr, 0.01 Mo, 1.32 Ni, 0.01 Al, 0.84 Cu and balance Fe. The *Butea monosperma* (Palash) leaves were dried in sunlight to remove moisture and powdered with the help of a grinder. The obtained powder was soaked in ethanol for a period of 24 h and then filtered using a Whatman filter paper No. 1. Ethanol was removed by vacuum evaporation to yield palash leaf extract (PLE).

Weight loss experiments were carried out as two sets, one employing modified Baar's medium containing SRB culture (UB) and the other with modified Baar's medium, SRB and 500 ppm PLE (IB). The abiotic experiments were performed by immersing the coupons in modified Baar's medium (U)/modified Baar's medium and 500 ppm PLE (I). The numbers at the end of U/UB and I/IB represents the immersion period in weeks. The metal coupons prepared for the studies were weighed and immersed in individual test tubes filled with the UB/IB medium and incubated at 37 °C. Total duration of the study was four weeks. To study the progress of corrosion, every week four samples were withdrawn and the weight of the samples after cleaning and drying was measured. The nutrient medium into which the respective samples were immersed was also analyzed for the dissolved sulfide concentration using the standard protocol.¹⁰ A comparison of the sample weight before and after immersion gives the weight loss of the sample, the average of which is used to estimate the corrosion rate CR using the method explained in the literature.¹ Similarly, for the electrochemical analysis techniques, the samples kept immersed were withdrawn from the media periodically for conducting potentiodynamic polarization (DP) and electrochemical impedance spectroscopy studies (EIS). Prior to each analysis, the samples were kept at open circuit potential (OCP) for 10 min. The scan rate used for DP was 5 mV/s. For EIS runs, the scan was done from 0.01 to 10³ Hz with an AC amplitude of 10 mV. The electrochemical techniques were performed at 37 °C on an electrochemical analyser (PARSTAT). An Ag/AgCl reference electrode and a platinum counter electrode were used for the studies. A scanning electron microscopy (SEM, Carl Zeiss UHR model) combined with an energy-dispersive X-ray system was used to study morphology and elemental composition of the samples. To study the various functional groups, present in the external film adhered to the surface of the sample Fourier transform infrared (FTIR) spectroscopy (Bruker, Alpha model) and X-ray photoelectron spectroscopy (XPS) were used. The composition of the PLE was found using a gas chromatography and mass spectrometry (GC-MS) unit (Agilent 5977).

RESULTS AND DISCUSSION

Weight loss study

The corrosion calculation by weight loss method was performed for stainless steel 202 coupons for a period of 28 days in both UB and IB media and the results are shown in Fig. 1a. In the UB sample, the CR of tested coupons was greater than in the IB medium. In the UB sample, the CR increases for the first two weeks and then remains stable till the fourth week. This could be due to the diffusion limitation caused by the deposition of corrosion products on the metal surface.

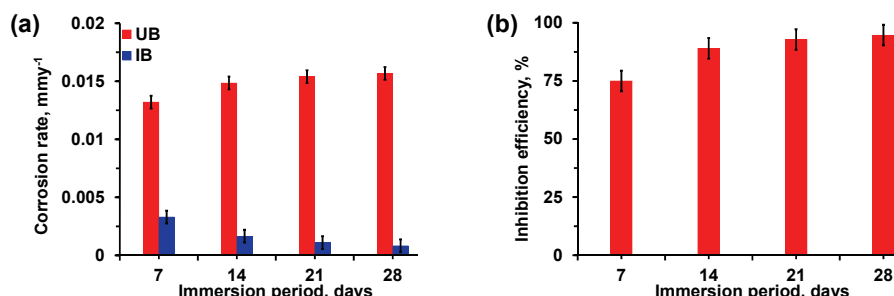


Fig. 1. a) Corrosion rate of stainless steel immersed in UB and IB medium and b) inhibition efficiency as a function of immersion period.

The CR of the IB sample presents a continuously decreasing trend indicating the formation of a stable, continuous external film that protects the surface. Fig. 1b shows the effect of the immersion period on the inhibition efficiency using 500 ppm of PLE. An average inhibition efficiency of 88 % was obtained.

Fig. S-1a and b of the Supplementary material to this paper show the corrosion rate of SS 202 in modified Baar's medium with (I) and without (U) Palash leaf extract in the absence of bacteria and inhibition efficiency as a function of immersion time, respectively. From Fig. 1a and S-1, it is clear that the corrosion rate in the abiotic case is significantly less when compared with the biotic case for both uninhibited and inhibited samples. The corrosion inhibition efficiency decreases with an increase in the immersion period, as seen in Fig. S-1b.

It is noteworthy to follow the sulfide concentration of the UB and IB samples during these periods which is presented in Fig. S-2 of the Supplementary material. During incubation the test tubes, containing UB and IB medium with SS samples immersed in them, turned black indicating the formation of iron sulfide set up by reaction between iron and HS⁻ caused by the SRB activity. The formation of H₂S is confirmed by the rotten egg odor upon opening the test tubes. From Fig. S-2, after the supplementation of the PLE, a decrease in dissolved sulfide content is clearly seen. This shows that the extract affects the metabolic activity of the bacteria resulting in reduced concentration of dissolved

sulfide. The literature suggests the neem leaf extract intervened in the metabolic activity of the *Desulfovibrio sp.* and inhibited the biocorrosion of API 5L X80 linepipe steel.¹¹ However, the palash leaf extract was reported for the inhibition of chemical corrosion of mild steel in HCl medium⁶ and not for biocorrosion except by our previous publication for galvanized steel.¹² The sulfide content in the UB sample increased from 48 ppm in the first week to 69 ppm in the fourth week. On the other hand, the IB sample showed a continuously decreasing trend in the sulfide values which ultimately goes to zero in the fourth week. There will be some variation in the bacterial count due to the death phase of the bacteria. The dissolved sulfide can also react with the metal and form metal sulfides. This is corroborated by the increase in the sulfide content of the UB sample. A similar trend in the sulfide concentration has been reported in the literature.¹³ Harrison and Thode studied the kinetic mechanism involved in the reduction of sulfate to sulfide by *D. desulfuricans* in Starkey's medium and optimized the temperature, metabolite concentrations and growth conditions.¹⁴ The literature is available with respect to the kinetic study of anaerobic reduction of sulfate to sulfide caused by the mixed consortium.¹⁵

Electrochemical impedance spectroscopy

The electrical characteristics of the biofilm and corrosion products layer can be analyzed using EIS. Fig. S-3 a and b of the Supplementary material show the impedance modulus measured at different frequencies in UB and IB samples at varied immersion times. Fig. S-3c and d show the phase angle variations with frequency for the same. From S-3a and c, it can be noticed that the addition of the inhibitor extract increases the impedance modulus approximately by ten times. The impedance modulus at low frequency for the UB sample decreases significantly during the third week and increases to a greater extent in the fourth week. This is due to the development of a thicker corrosion products film during the fourth week which prevents the movement of the electrolyte. In the case of IB samples, the maximum impedance modulus at low frequency is observed for the third week. This decreases again in the fourth week which is due to the change in the thickness and composition of the external film formed on the metal. The formation of a thicker corrosion products layer during third week in IB sample matches well with the SEM findings. Overall, the impedance modulus of the IB samples is approximately ten-times higher at low frequencies for all the immersion durations indicating higher resistance to material degradation. The Bode phase angle plot shows the presence of two-time constants in both cases. In the case of UB samples, the phase angle at the lowest frequency decreases for the second and third weeks indicating an increase in corrosion. For the fourth week, the low-frequency peak is broader and shows a shift towards low frequency

which indicates good adsorption of the external film on the metal surface which offers protection against corrosion.¹⁶

In the case of IB samples, the phase angle peak at low frequency increases slightly for the second week. For the third week, the phase angle peak at the lower frequency region is much broader when compared to other weeks. The impedance modulus plot for the same period shows a maximum value at the lowest frequency which indicates that the film formed during the third week is continuous with good corrosion protection. Similarly, for the fourth week, the phase angle peak shows a shift towards lower frequency accompanied by an increase in peak value indicating good corrosion protection with immersion time.¹⁶

Fig. 2a and b illustrate the Nyquist plot for the SS sample in UB and IB media at different times. The high-frequency zone presents a semi-circular pattern and the low-frequency region shows the presence of diffusion limitation. The high-frequency semi-circular pattern shows the features of a depressed semicircle which is caused by surface roughness. Hence the system is modeled with a constant phase element (CPE) instead of an ideal capacitor. The impedance of any CPE element "i" (Z_i) is given as:

$$Z_{i\text{CPE}} = Y_i^{-1} (j\omega)^{-n} \quad (1)$$

In the above equation, Y_i is the admittance in $\text{S s}^n \text{ cm}^{-2}$, ω is the angular frequency in rad s^{-1} , j is -1 and n is the roughness parameter the value of which becomes 1 for an ideal capacitor.

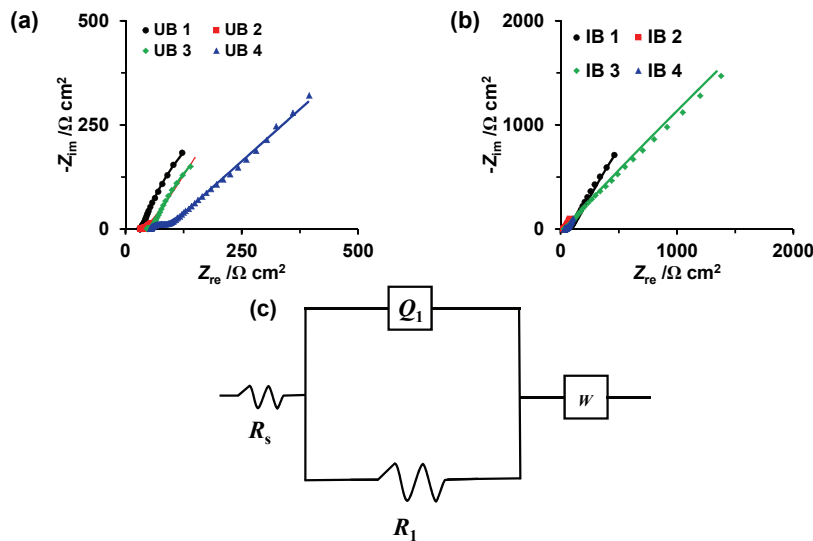


Fig. 2. Nyquist plot for stainless steel in: a) UB and b) IB medium. The experimental data is represented using a continuous line and dots depict equivalent electrical circuit (EEC) fit. c) EEC used for fitting the EIS data.

The equivalent circuit used to model the system is represented in Fig. 2c. The CPE is represented by Q_1 and the diffusion element is represented using Warburg impedance (W). The impedance (Z_W) of the Warburg diffusion element is given as:¹⁷

$$Z_W = Y_0^{-1} (2\omega)^{-0.5} (1-j) \quad (2)$$

where Y_0 is the admittance in $S s^n cm^{-2}$, ω is the angular frequency in $rad s^{-1}$.

Table I shows the best-fit parameters obtained for the EEC. The continuously decreasing trend of R_1 , with immersion time in the case of the UB sample, and the continuously increasing trend of the same with immersion time for the IB sample match well with the results obtained from the weight loss studies. The capacitance (C_1) of the CPE element can be found from the admittance Y_1 , resistance R_1 associated with the CPE unit, and the corresponding roughness parameter n_1 calculated using:¹⁸

$$C_1 = (Y_1 (R_1^{1-n_1}))^{1/n_1} \quad (3)$$

The capacitance values are inversely proportional to the film thickness.² The calculated capacitance values in Table I show that the thickness of the film in the UB sample increases with immersion time while the inhibited sample presents a stable capacitance value which shows that the external film thickness is not altered significantly with immersion time.

TABLE I. EEC fitted value for the stainless steel in biotic and inhibited cases

Parameter	Biotic (UB)				Inhibitor (IB)			
	UB 1	UB 2	UB 3	UB 4	IB 1	IB 2	IB 3	IB 4
$R_s / \Omega cm^2$	31.26	37.34	49.67	53.8	53.19	29.03	33.81	38.59
$Y_1 \times 10^4 / S s^n cm^{-2}$	765	2290	1576	3	138	75	100	125
n_1	0.9187	1	1	0.6441	1	0.9007	0.9504	1
$R_1 / \Omega cm^2$	654.3	543.8	320.1	33.52	2061	2402	2581.5	2761
$W \cdot Y_0 / S s^{0.5} cm^{-2}$	0.0803	0.0272	0.0464	0.0082	0.0047	0.0102	0.0080	0.0059
$C_1 / \mu F cm^{-2}$	0.24	0.23	0.16	0.004	0.01	0.03	0.02	0.01

The inverse of Warburg admittance gives the resistance offered by the diffusion barrier. It is clearly seen that the diffusion resistance offered by the barrier is high with the PLE inhibitor.

Potentiodynamic polarization study (Tafel)

Tafel plot for the SS sample in UB and IB media after immersion for defined durations (up to four weeks) is shown in Fig. S-4 of the Supplementary material. The Tafel parameters obtained by Tafel region extrapolation are listed in Table II. It can be seen that the E_{corr} shows a positive shift with the immersion period in both UB and IB samples. This shows the formation of passive layer which pre-

vents the diffusion of the corrosive medium. When inhibitor molecules are added to the aggressive medium, the cathodic reaction is slowed, resulting in a negative shift in the open circuit potential observed for the first week which could be attributed to the decreased hydrogen generation at the cathode due to the adsorption of the inhibitor molecules.^{19,20} Potentiodynamic polarization plots show a significant change with the addition of an inhibitor and hence alter the mechanism of hydrogen generation and anodic dissolution reactions.^{1,21,22} From the second week positive shift in the potential with inhibitor addition can be observed. Moreover, it is clearly observed that both the cathodic and the anodic current densities are drastically decreased with the inhibitor addition. This gives information that both the cathodic hydrogen generation and anodic dissolution reactions are affected with the inhibitor addition. Thus, the inhibitor acts as a mixed inhibitor. Previously, the sulfide analysis results indicated that the inhibitor affected the metabolic activities of the SRB. Thus, the inhibitor works as a corrosion inhibitor and also as an antibacterial agent. Moreover, the j_{corr} values are lowered with the addition of the inhibitor and with immersion time it shows a continuously decreasing trend which shows the improved corrosion resistance properties of the inhibitor layer with time. In the absence of the inhibitor continuously increasing trend in the same can be observed. On the other hand, a continuously decreasing tendency is observed for j_{corr} with the inhibitor extract. As the stainless steel 202 grade contains manganese instead of nickel, the j_{corr} values are higher. Vignesh *et al.* reported j_{corr} value of 246.1 $\mu\text{A cm}^{-2}$ for SS202 in NaCl medium.²³

TABLE II. Tafel fit parameters for stainless steel in biotic (a) and inhibited (b) to study various parameter to study biocorrosion

Sample		E_{corr} V vs. Ag/AgCl	j_{corr} $\mu\text{A cm}^{-2}$	b_a mV dec ⁻¹	$-b_c$ mV dec ⁻¹	CR mm y ⁻¹	IE %
Biotic (UB)	UB1	-0.58	78	88.19	48.69	0.83	—
	UB2	-0.51	92.6	164.55	87.21	0.98	—
	UB3	-0.41	137	220	157.38	1.45	—
	UB4	-0.33	197.6	208.32	119.07	2.10	—
Inhibitor (IB)	IB1	-0.82	14.2	176	92.57	0.15	81.8
	IB2	-0.35	9.3	157	96.27	0.10	90.1
	IB3	-0.28	4.5	79.62	55.5	0.05	96.7
	IB4	-0.09	3.7	142.36	102.58	0.04	98.1

FTIR analysis

Fig. 3a–c shows the FTIR spectra for the samples immersed in the UB and IB media along with the spectrum of the Palash leaf extract. The FTIR spectrum of samples in the UB medium show strong peaks between 650–660 cm^{-1} which correspond to the presence of the acetal group, one of the major components of

the bacterial biofilm.²⁴ The peak at 1500–1520 cm⁻¹ corresponds to the amide II functional groups (NH bending and CN stretching) in the biofilm.²⁵ The peak at 2353 cm⁻¹ corresponds to N–H or C=O stretching vibrations.²⁶ The peak at 3737 cm⁻¹ corresponds to the hydroxyl groups of the biofilms.²⁷ The samples immersed in IB samples show the presence of amide II functional groups (1530 cm⁻¹) and esters (1680–1700 cm⁻¹). Apart from that peak at 2353 cm⁻¹ corresponding to N–H or C=O group can also be observed. The sample also shows the presence of O–H group (3740 cm⁻¹).

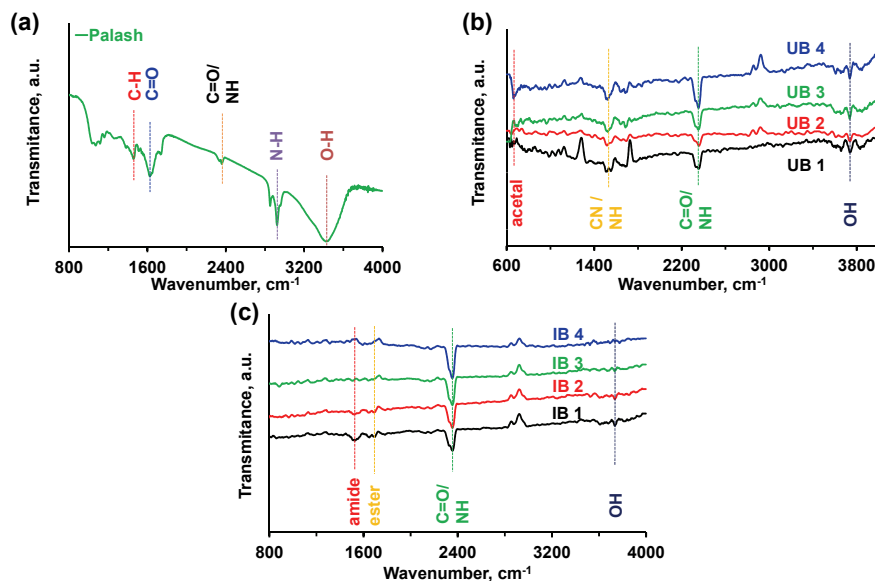


Fig. 3. FTIR analysis of ethanolic extract of: a) Palash leaf extract, b) biotic case and c) inhibited case in the medium.

Scanning electron microscopy

The SEM images of the UB and IB samples with the external film formed on them after one and three weeks of immersion period are shown in Fig. 4. The UB sample at the end of first week shows many sessile cells with two distinct layers - One compact inner layer and an outer layer that shows spherical structures scattered all over the sample surface. The third-week UB sample shows the presence of numerous sessile bacteria and a compact external biofilm layer. The compactness of the external layer in the case of UB sample increases with the immersion period which adds strength to the weight loss results where the corrosion rate stays stable after two weeks of immersion. The IB sample shows the presence of a very thin external layer in the first week. In the third week's sample, tiny scattered granular structures can be observed which could be due to the adsorbed cor-

rosion products and inhibitor molecules. Table S-I of the Supplementary material shows the elemental composition of the UB and IB samples at different immersion period. The IB samples show higher carbon content when compared to UB samples which could be due to the adsorbed inhibitor molecules. The sulfide and iron concentrations are high in the UB samples due to the formation and deposition of iron sulfide.

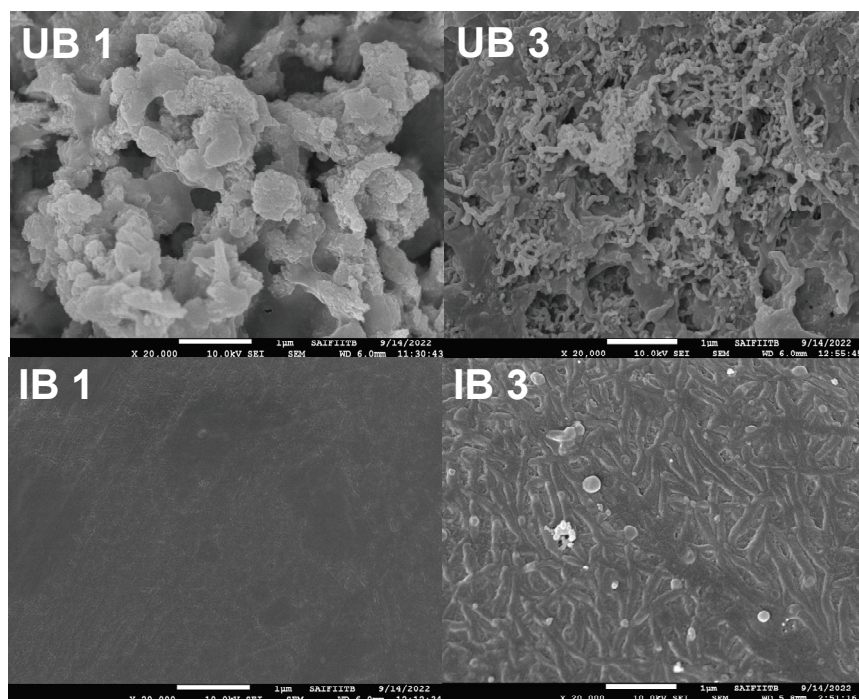


Fig. 4. SEM images of the layer formed on the stainless-steel coupons immersed in UB and IB medium for 1- and 3-week immersion periods.

GC–MS analysis

The findings of the GC–MS analysis of PLE are given in Table S-II of the Supplementary material. The analysis shows that about 78.9 % of the extract is composed of terpenoids which are known for their antioxidant and antibacterial properties. Similarly, compounds such as vitamin E and W-18 are also helpful in controlling bacterial growth and corrosion.

X-ray photoelectron spectroscopy

Fig. 5a–e show the deconvoluted XPS spectra for the elements: iron, nitrogen, carbon, oxygen and sulfur, respectively. The Fe2p deconvolution peak at 706.6 eV confirms the presence of FeS_2 .²⁸ The peaks at 710.8 and 716.6 eV arise

due to the presence of Fe^{3+} . The presence of metallic Fe is denoted by the peak at 719.2 eV.²⁰ The N1s deconvolution gives two peaks one at 399.4 eV and the second at 400.7 eV. These belong to the amine groups of the biological system.²⁹ The deconvoluted C1s spectra for the third week UB sample with an external film formed on it shows peaks at 284.1, 285.6 and 287.6 eV corresponding to C=C, C-C, O-C-O and C=O functional groups, respectively.³⁰ These peaks are contributions from the organic compounds present in the biofilm. The O1s spectra for the UB sample show two significant peaks at 531.3 and 530.9 eV corresponding to carbonyl compounds of biofilm and the iron oxides formed due to corrosion reactions.³¹ The S2p deconvolution shows a peak at 163.5, 166.6 and 168.6 eV corresponding to the presence of iron sulfide ($\text{Fe}_{0.89}\text{S}$), SO_3 and SO_4^{2-} , respectively.³²⁻³⁴

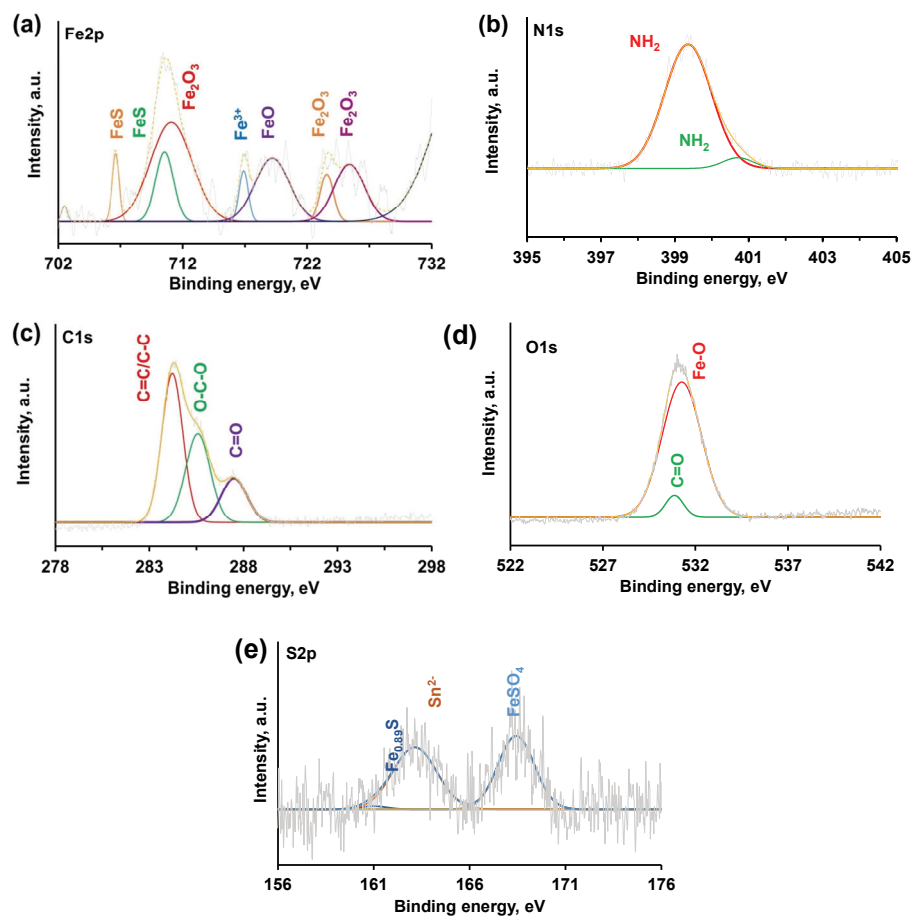


Fig. 5. Deconvoluted XPS spectra of SS 202 in UB medium: a) Fe2p, b) N1s, c) C1s, d) O1s and e) S2p.

Fig. 6a–e shows the deconvoluted XPS spectra of various elements in IB sample. The C1s spectra show the presence of C=C (284.3 eV) which could be a contribution from inhibitor component W-18.^{30,35} The peak at 285.7 eV corresponds to C–O group. The O1s deconvolution gives peak at 530.6 eV which represents iron oxides and the peak at 531.5 eV affirms the presence of organic C–O bond.³⁶ The N1s deconvolution shows primary peak at 398.3 eV that is characteristic of pyridinic group which could have come from the W-18 compound of the inhibitor extract.³⁷ The peaks at 399.9 and 402.4 eV signify amide and N–O groups, respectively.^{38,39} The peak at 407.9 eV corresponds to NO₃⁻.⁴⁰ The peaks at 709.4 and 723 eV, and the satellite peak at 715.3 eV show the presence of Fe²⁺.⁴¹ The peak at 160.8 eV in the deconvoluted s2p spectra shows the existence of S²⁻ and the peaks at 162.4 and 169 eV, respectively, show the presence of S₂²⁻ and SO₄²⁻.⁴² The sulfide group could have originated from the sulfonamide products of inhibitor molecules or from FeS. The products of corrosion from the XPS studies based on literature include iron sulfides and oxides.

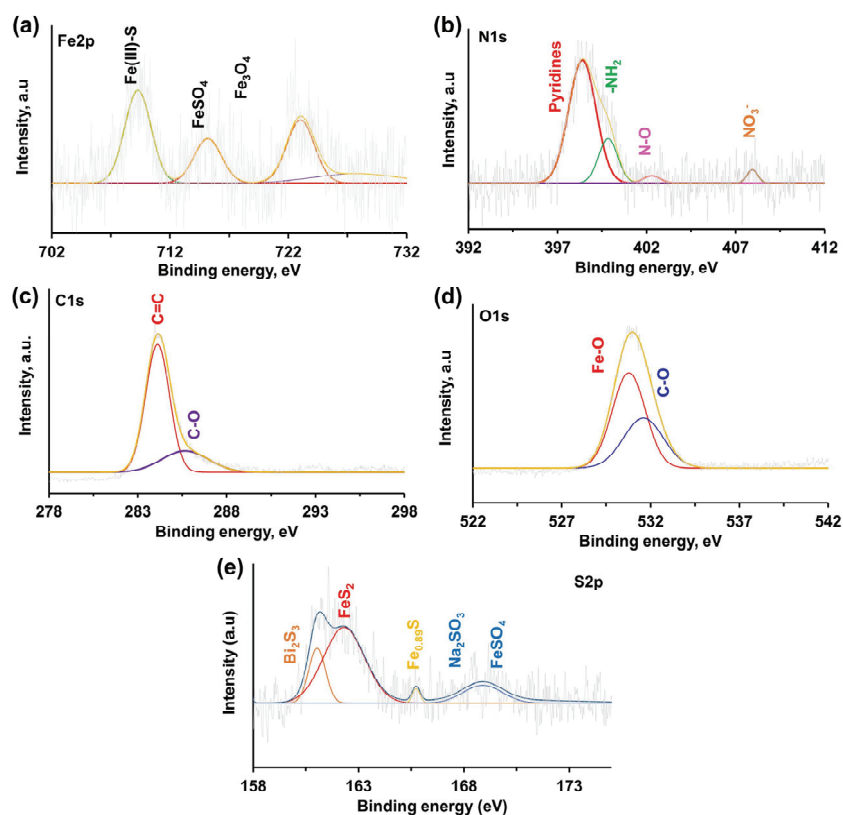
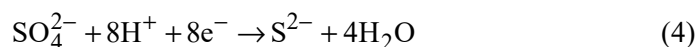


Fig. 6. Deconvoluted XPS spectra of SS 202 in IB medium: a) Fe2p, b) N1s, c) C1s, d) O1s and e) S2p.

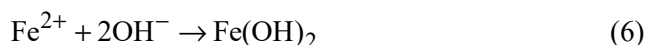
Table S-I shows the elemental composition of the samples analyzed by EDAX. The increased amount of carbon in the inhibited sample is due to the adsorbed inhibitor molecules. The sulfide and iron content are very low in the IB sample.

Mechanism

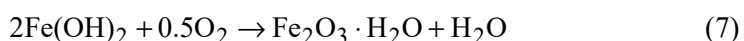
Analysis of the external film formed on the UB and IB samples have shown that the samples mainly consisted of iron sulfides and oxides. The dissolution of iron in SS 202 causes formation of Fe^{2+} . The SRB utilize the hydrogen ions generated by the water dissociation, sulfate in the environment and the electrons from iron dissolution for the reduction reaction to produce FeS .^{43,44} The following reactions can be written:



Apart from the formation of FeS , the hydroxyl radicals formed from water dissociation react with Fe^{2+} to yield Fe(OH)_2 :



In the alkaline environment the Fe(OH)_2 reacts to give rust ($\text{Fe}_2\text{O}_3 \cdot \text{H}_2\text{O}$):^{43,45}



The sulfides produced by SRB are more reactive, soluble and exist in more reduced form. In the present study pH measurement after four weeks shows a pH close to 9. At these alkaline conditions, the sulfides produced easily react to produce polysulfides and sulfur.^{46,47} With the inhibitor extract the number of sessile bacteria is reduced as observed from the SEM images and the metabolic activity of the bacteria is also decreased which is reflected in the decreased dissolved sulfide concentration, corrosion products and corrosion rate.

CONCLUSIONS

The effect of palash leaf extract in the control of SRB caused corrosion in SS 202 was studied in detail. Over an immersion period of four weeks, 500 ppm of PLE was able to control the corrosion by 88 %. The SEM analysis showed the formation of different kinds of external layer on the sample in the presence and absence of PLE. In the case of uninhibited samples, the biofilm thickness and the number of sessile bacteria increased with immersion period. In the inhibited sample a very thin external film was observed. The XPS analysis showed significant products of corrosion as FeS and Fe_2O_3 . The inhibitor consisted of 78 % terpenoids which are known for their antioxidant and antibacterial effects. The

PLE was found to work well in the control of SS 202 corrosion caused by SRB activity in the neutral medium.

SUPPLEMENTARY MATERIAL

Additional data and information are available electronically at the pages of journal website: <https://www.shd-pub.org.rs/index.php/JSCS/article/view/12207>, or from the corresponding author on request.

ИЗВОД

ИСПИТИВАЊЕ ИНХИБИТОРСКИХ КАРАКТЕРИСТИКА ЕКСТРАКТА ЛИШЋА *Butea monosperma* НА УСПОРАВАЊЕ БИОКОРОЗИЈЕ НЕРЂАЈУЋЕГ ЧЕЛИКА У ПРИСУСТВУ СУЛФАТ-РЕДУКУЈУЋИХ БАКТЕРИЈА

SHIV KUMAR MANU, NOYEL VICTORIA SELVAM и MANIVANNAN RAMACHANDRAN

Department of Chemical Engineering, National Institute of Technology Raipur, Chhattisgarh – 492010, India

Утицај сулфат-редукујућих бактерија *Desulfovibrio desulfuricans* на корозију нерђајућег челика SS 202 у неутралној средини је детаљно испитиван коришћењем методе губитка масе и електрохемијских метода. Активност бактерија доводи до губитка материјала просечном брзином од 0,015 mm/год. Анализа скенирајућом електронском микроскопијом (СЕМ) је показала значајан пораст популације сесилних бактерија током периода урењања. Примена екстракта лишћа биљке шумски пламен (*Butea monosperma*) концентрације 500 ppm је смањила просечну брзину корозије на 0,002 mm/год. СЕМ анализом је показано да се у присуству инхибитора формира веома танак спољашњи филм. Фотоелектронска спектроскопија X-зрацима је потврдила присуство корозионих продуката као што су Fe₂O₃ и FeS. Испитивањима гасном хроматографијом–масеном спектрометријом је утврђено да су главне компоненте екстракта листа шумског пламена различити терпеноиди и витамин E. Електрохемијска анализа је показала присуство дифузионе баријере током корозије. Отпорност која потиче од дифузионе баријере се значајно повећава у присуству инхибитора.

(Примљено 30. децембра 2022, ревидирано 10. јануара, прихваћено 12. маја 2023)

REFERENCES

1. A. Sharma, M. Ramachandran, N. V. Selvam, *Corr. Rev.* **40** (2021) 87 (<https://doi.org/10.1515/corrrev-2021-0019>)
2. B. S. Swaroop, S. N. Victoria, R. Manivannan, *J. Taiwan Inst. Chem. Eng.* **64** (2016) 269 (<https://doi.org/10.1016/j.jtice.2016.04.007>)
3. Y. Y. Yong, G. A. Dykes, W. S. Choo, *Crit. Rev. Microbiol.* **45** (2019) 201 (<http://doi.org/10.1080/1040841X.2019.1573802>)
4. M. M. Cowan, *Clin. Microbiol. Rev.* **12** (1999) 564 (<https://doi.org/10.1128/CMR.12.4.564>)
5. L. Lu, W. Hu, Z. Tian, D. Yuan, G. Yi, Y. Zhou, *Chin. Med.* **14** (2019) 11 (<http://doi.org/10.1186/s13020-019-0232-2>)
6. A. Singh, M. A. Quraishi, E. E. Ebenso, *Int. J. Electrochem. Sci.* **7** (2012) 12545 (<http://www.electrochemsci.org/papers/vol7/71212545.pdf>)
7. M. C. Sahu, R.N. Padhy, *Asian Pac. J. Trop. Dis.* **3** (2013) 217 ([https://doi.org/10.1016/S2222-1808\(13\)60044-4](https://doi.org/10.1016/S2222-1808(13)60044-4))
8. J. Tao, S. Yan, H. Wang, L. Zhao, H. Zhu, Z. Wen, *LWT* **154** (2022) 112631, (<https://doi.org/10.1016/j.lwt.2021.112631>)

9. Y. Lekbach, Y. Dong, Z. Li, D. Xu, S. El Abed, Y. Yi, L. Li, S. I. Koraichi, T. Sun, F. Wang, *Corros. Sci.* **157** (2019) 98 (<https://doi.org/10.1016/j.corsci.2019.05.021>)
10. *ASTMG31-12a, Standard Guide for Laboratory Immersion Corrosion Testing of Metals*, 2012 (<http://www.astm.org/Standards/G31>)
11. S. M. Bhola, F. M. Alabbas, R. Bhola, J. R. Spear, B. Mishra, D. L. Olson, A. E. Kakpovbia, *Eng. Fail. Anal.* **36** (2014) 92 (<https://doi.org/10.1016/j.engfailanal.2013.09.015>)
12. S. K. Manu, S. N. Victoria, R. Manivannan, *J. Indian Chem. Soc.* **99** (2022) 100652 (<https://doi.org/10.1016/j.jics.2022.100652>)
13. S. Kebbouche-Gana, M.L. Gana, *Ann. Microbiol.* **62** (2012) 203 (<https://doi.org/10.1007/s13213-011-0247-0>)
14. A.G. Harrison, H.G. Thode, *Trans. Faraday Soc.* **54** (1958) 84 (<https://doi.org/10.1039/TF9585400084>)
15. S. Moosa, M. Nemat, S. T. L. Harrison, *Chem. Eng. Sci.* **57** (2002) 2773 ([https://doi.org/10.1016/S0009-2509\(02\)00152-5](https://doi.org/10.1016/S0009-2509(02)00152-5))
16. S. Meng, Z. Liu, X. Zhao, B. Fan, H. Liu, M. Guo, H. Hao, *RSC Adv.* **11** (2021) 31693 (<https://doi.org/10.1039/d1ra04976c>)
17. C. N. Cao, J. Q. Zhang, *An Introduction to Electrochemical Impedance Spectroscopy*, Science Press, Beijing, 2002
18. H. Ma, X. Cheng, G. Li, S. Chen, Z. Quan, S. Zhao, L. Niu, *Corros. Sci.* **42** (2000) 1669 ([https://doi.org/10.1016/S0010-938X\(00\)00003-2](https://doi.org/10.1016/S0010-938X(00)00003-2))
19. R. S. Abdel Hameed, *Int. J. Electrochem. Sci.* **17** (2022) 221017 (<https://doi.org/10.20964/2022.10.31>)
20. Y. Guo, T. Meng, D. Wang, H. Tan, R. He, *Eng. Fail. Anal.* **78** (2017) 87 (<https://doi.org/10.1016/j.engfailanal.2017.03.003>)
21. H. Liu, G. Meng, W. Li, T. Gu, H. Liu, *Front. Microbiol.* **10** (2019) 1298 (<https://doi.org/10.3389/fmicb.2019.01298>)
22. G. Vignesh, C. S. Narayanan, P. Chinnaiyan, K. Shanmugapriya, *Mater. Res. Express* **6** (2019) 126540 (<https://doi.org/10.1088/2053-1591/ab5606>)
23. A. Kumar, P.C. Srivastava, *Mater. Sci.-Pol.* **37** (2019) 116 (<https://doi.org/10.2478/msp-2019-0001>)
24. C. Mayer, R. Moritz, C. Kirschner, W. Borchard, R. Maibaum, J. Wingender, H. C. Flemming, *Int. J. Biol. Macromol.* **26** (1999) 3 ([https://doi.org/10.1016/S0141-8130\(99\)00057-4](https://doi.org/10.1016/S0141-8130(99)00057-4))
25. A. Z. M. Rus, in *Biopolymers and biotech admixtures for eco-efficient construction materials*, F. Pacheco-Torgal, V. Ivanov, N. Karak, H. Jonkers, Eds., Woodhead Publishing, Sawston, 2016, p. 427 (<https://doi.org/10.1016/C2014-0-02075-8>)
26. S. Vijayakumar, B. Vaseeharan, B. Malaikozhundan, N. Gopi, P. Ekambaram, R. Pachaiappan, P. Velusamy, K. Murugan, G. Benelli, R. S. Kumar, M. Suriyanarayananamoorthy, *Microbial Pathogenesis* **102** (2017) 173 (<https://doi.org/10.1016/j.micpath.2016.11.029>)
27. M. M. Haque, M. K. Mosharaf, M. A. Haque, M. Z. H. Tanvir, M. K. Alam, *Front. Microbiol.* **12** (2021) 615113 (<https://doi.org/10.3389/fmicb.2021.615113>)
28. H. Qi, Y. Wang, J. Feng, R. Peng, Q. Shi, X. Xie, *Int. J. Environ. Res. Public Health* **19** (2022) 15416 (<https://doi.org/10.3390/ijerph192215416>)
29. P. Li, M. Yu, X. Ke, X. Gong, Z. Li, X. Xing, *ACS Appl. Bio Mater.* **5** (2022) 3290 (<https://doi.org/10.1021/acsabm.2c00292>)

30. H.-W. Tien, Y.-L. Huang, S.-Y. Yang, J.-Y. Wang, C.-C. M. Ma, *Carbon* **49** (2011) 1550 (<https://doi.org/10.1016/j.carbon.2010.12.022>)
31. N. Sarmadi, M. Gharabaghi, M. T. Saray, M. Darestani, D. Garman, P. Koshy, S. S. Mofarah, C. C. Sorrell, *Inorg. Chem.* **60** (2021) 175 (<https://dx.doi.org/10.1021/acs.inorgchem.0c02762>)
32. Y. Yuan, L. Wang, L. Gao, *Front. Chem.* **8** (2020) 818 (<https://doi.org/10.3389/fchem.2020.00818>)
33. M. Watanabe, H. Ando, T. Handa, T. Ichino, N. Kuwaki, *Zairyo-to-Kankyo* **56** (2007) 10 (<https://doi.org/10.3323/jcorr.56.10>)
34. *NIST X-ray Photoelectron Spectroscopy Database*, 2012 (<http://dx.doi.org/10.18434/T4T88K>)
35. E. E. Knaus, B. K. Warren, T. A. Ondrus (University of Alberta, Bayer Corp) US Patent Publication 4,468,403 (1984)
36. Y. Wu, Y. Lin, J. Xu, *Photochem. Photobiol. Sci.* **18** (2019) 1081 (<https://doi.org/10.1039/C8PP00493E>)
37. D. Kim, Y. Kwon, J.-H. Lee, S.-J. Kim, Y.-I. Park, *Membranes* **12** (2022) 93 (<https://doi.org/10.3390/membranes12010093>)
38. R. J. J. Jansen, H. van Bekkum, *Carbon* **33** (1995) 1021 ([https://doi.org/10.1016/0008-6223\(95\)00030-H](https://doi.org/10.1016/0008-6223(95)00030-H))
39. X. Yan, T. Xu, G. Chen, S. Yang, H. Liu, Q. Xue, *J. Phys., D* **37** (2004) 907 (<https://doi.org/10.1088/0022-3727/37/6/015>)
40. Y. R. Park, M. J. Ko, Y.-H. Song, C. J. Lee, *J. Appl. Phys.* **114** (2013) 153516 (<https://doi.org/10.1063/1.4826206>)
41. G. Dong, M. Fang, J. Zhang, R. Wei, L. Shu, X. Liang, S. Yip, F. Wang, L. Guan, Z. Zheng, J. C. Ho, *J. Mater. Chem., A* **5** (2017) 11009 (<https://doi.org/10.1039/C7TA01134B>)
42. Z. Otgonbayar, W. C. Oh, *J. Inorg. Organomet. Polym.* **32** (2022) 2910 (<https://doi.org/10.1007/s10904-022-02319-8>)
43. V. C. Nettikaden, D. Ifezue, F. H. Tobins, *J. Fail. Anal. Preven.* **14** (2014) 43 (<https://doi.org/10.1007/s11668-013-9757-3>)
44. F. Guan, X. Zhai, J. Duan, M. Zhang, B. Hou, *PLoS One* **11** (2016) e0162315. (<https://dx.doi.org/10.1371/journal.pone.0162315>)
45. Z. Ahmad, *Principles of Corrosion Engineering and Corrosion Control*, Butterworth-Heinemann, Oxford, 2006 (<https://doi.org/10.1016/B978-0-7506-5924-6.X5000-4>)
46. S. L. Johnston, G. Voordouw, *Environ. Sci. Technol.* **46** (2012) 9183 (<https://doi.org/10.1021/es3019594>)
47. R. Cord-Ruwisch, W. Kleinitz, F. Widdel, *J. Pet. Technol.* **39** (1987) 97 (<https://doi.org/10.2118/13554-PA>).